Infinite boundary conditions for matrix product state calculations

Ho N. Phien,[1] Guifré Vidal,[2] and Ian P. McCulloch[1]

[1]*Centre for Engineered Quantum Systems, School of Mathematics and Physics, University of Queensland, Brisbane 4072, Australia*

[2]*Perimeter Institute for Theoretical Physics, Waterloo, Ontario, Canada N2L 2Y5*

(Received 23 July 2012; revised manuscript received 29 November 2012; published 10 December 2012)

We propose a formalism to study dynamical properties of a quantum many-body system in the thermodynamic limit by studying a finite system with "infinite boundary conditions" where both finite-size effects and boundary effects have been eliminated. For one-dimensional systems, infinite boundary conditions are obtained by attaching two boundary sites to a finite system, where each of these two sites effectively represents a semi-infinite extension of the system. One can then use standard finite-size matrix product state techniques to study a region of the system while avoiding many of the complications normally associated with finite-size calculations such as boundary Friedel oscillations. We illustrate the technique with an example of time evolution of a local perturbation applied to an infinite (translationally invariant) ground state, and use this to calculate the spectral function of the $S = 1$ Heisenberg spin chain. This approach is more efficient and more accurate than conventional simulations based on finite-size matrix product state and density-matrix renormalization-group approaches.

DOI: 10.1103/PhysRevB.86.245107 PACS number(s): 03.67.−a, 03.65.Ud, 02.70.−c, 05.30.Fk

I. INTRODUCTION

In recent decades, the tensor network formalism has emerged as a set of powerful numerical techniques to investigate physical properties of strongly correlated quantum many-body systems. For instance, in 1D systems, the density-matrix renormalization group (DMRG)[1,2] is probably the single most powerful method to compute numerically exact ground states. Furthermore, the development of the time-evolving block decimation (TEBD) algorithm[3,4] highlighted the great advantages of the matrix product state (MPS)[5–7] representation, which incorporates DMRG and TEBD into the same framework.[8,9] Meanwhile, tensor product state (TPS)[10–15] and projected entangled-pair state (PEPS)[16–18] methods are developing into important tools for the study of 2D systems.

For calculating bulk properties of matter, it is desirable to take the thermodynamic limit and avoid the influence of boundary conditions. In many methods, the thermodynamic limit is not possible to study directly, but instead requires the extrapolation of results for increasingly larger system sizes. This is because for most algorithms the computational cost increases with the system size; however approaching the thermodynamic limit in this way is computationally expensive. In 1D, there exist algorithms that overcome this limit by taking advantage of the invariance under translation in space. One of these is the infinite time-evolving block decimation (iTEBD),[19,20] originally introduced to investigate the time evolution problem for infinite-size 1D spin chains. In this algorithm, the infinite MPS (iMPS) is represented by a small set of tensors which are invariant under translation of one unit cell (equal to two sites for the usual TEBD scheme). This algorithm can be used to obtain a translationally invariant ground state by evolving the tensors in imaginary time until the fixed point is reached. The resulting iMPS is not only a good representation of ground state, but compared with finite MPS the number of wave function parameters is reduced and the iMPS form is very convenient for calculating observables of the system in the thermodynamic limit. The iTEBD algorithm is very easy to implement; however there are many ways to optimize an iMPS to achieve the same fixed point. A faster converging algorithm which also allows more flexibility in the size of the unit cell is the iDMRG[21,23] algorithm, but other algorithms exist with some advantages for some situations.[24,25]

Although the iMPS representation of a wave function is very useful for studying physical systems in the thermodynamic limit, there are some applications for which breaking of translational invariance is essential, such as the response to a local perturbation. The time evolution of a local perturbation is a common technique used in MPS calculations to obtain the spectral function[8,26] which to date has required using a finite MPS representation. However, the use of a finite MPS has several disadvantages. In particular, the system size needs to be large enough that the excitation is not influenced by the boundary of the system. This clearly requires that the propagating excitation will not hit the boundary, but even this is not enough since the boundary will induce inhomogeneities such as Friedel oscillations, which means that the system size must be quite large even to obtain an approximately homogeneous ground state in the central region of the lattice.

The notion of translational invariance of an iMPS can be generalized to states with finite momentum, whereby instead of requiring invariance under some number of lattice shifts, we instead require only that the iMPS is an eigenstate of translations with some complex eigenvalue e^{ik} representing the momentum. The resulting iMPS remains *position independent* but is constructed in such a way that the transfer operator has nontrivial phase factors. Algorithms have been proposed for expectation values[5,27] and quasiparticle excitations[28] using this scheme.

For infinite-size systems an equivalent problem was also investigated in Ref. 29. In that work the authors proposed an efficient method to simulate both imaginary- and real-time evolution of the infinite-size system with impurities by transversely contracting the tensor networks along the space direction rather than along the time direction as in standard iTEBD. By using a folding technique to reduce the entanglement of the MPS representation the transverse contraction approach can achieve longer times than other techniques; nevertheless it cannot avoid some drawbacks. For instance, by employing the

Suzuki-Trotter decomposition[30] in the evolution operator with small time step, the finite number of rows along the time axis may be very large. This may cause difficulty in finding the left and right dominant eigenvectors of the transfer matrix.

We will investigate the above problem in a different way by introducing what we call *infinite boundary conditions* for a finite MPS. We begin with the ground state of a many-body 1D system described by an iMPS. A finite region of the infinite system can be perturbed while still utilizing the iMPS structure for the tensors not directly affected by the perturbation. The resulting structure is equivalent to a finite MPS with a specially constructed "pseudosite" at each end which effectively represents an infinite extension of the system. A key point of this construction is that the Hilbert space for the infinite extension is fixed but the wave function is not; hence it can freely explore all of the available states in the effective Hilbert space of the infinite extension. The result is that, in contrast to conventional finite-size MPS calculations where a propagating excitation reaching the boundary of the system will reflect back, in our scheme an excitation can propagate off the end of the finite MPS. As long as the perturbation outside the finite boundary is not too big there is little loss in fidelity from allowing it to do so.

The evolution of a finite section of an iMPS was considered by Kjäll *et al.*,[31] who used this notion in obtaining the time evolution of a translationally invariant state that had been perturbed by a local particle excitation. However their scheme was rather specific to the particular setting, of Suzuki-Trotter-based real-time evolution. In this paper we show that this idea can be taken much farther, and by mapping the problem onto a finite MPS then *any* algorithm for finite MPS calculations can be applied to an infinite system.

The paper is organized as follows: In Sec. II we will introduce the infinite boundary condition definition and effective Hamiltonian calculation. In Sec. III we review the problem of a local perturbation in the infinite spin chain and real-time evolution algorithm. In Sec. IV we then apply the idea of infinite boundary conditions to simulate the time evolution of the spin-1 isotropic antiferromagnetic Heisenberg model. The results are presented by calculating time-dependent observables such as local magnetization $\langle S_z(x,t)\rangle$ to see how a wave front propagates in time and unequal-time two-point correlator $A(x,t)$, from which we can extract the spectral function and dispersion relation of the system. Finally, Sec. V contains our conclusions.

II. INFINITE BOUNDARY CONDITIONS

A. Formulation

Let us consider an infinite-size spin chain for which the wave function is described by a one-site translationally invariant canonical iMPS

$$|\Psi\rangle = \sum_{\{s_i\}} \ldots \lambda\Gamma^{s_{i-1}}\lambda\Gamma^{s_i}\lambda\Gamma^{s_{i+1}}\lambda\Gamma^{s_{i+2}} \ldots |\mathbf{s}\rangle, \qquad (1)$$

where $|\mathbf{s}\rangle = |\ldots s_{i-1}, s_i, s_{i+1}, s_{i+2}\ldots\rangle$; s_i is the local index that represents an element in local Hilbert space at the ith site of the spin chain. The matrices Γ^s and λ have dimension $\chi \times \chi$ and λ is diagonal. Notice that while the notation of bond dimension is usually used as m or D in the DMRG language, here we use

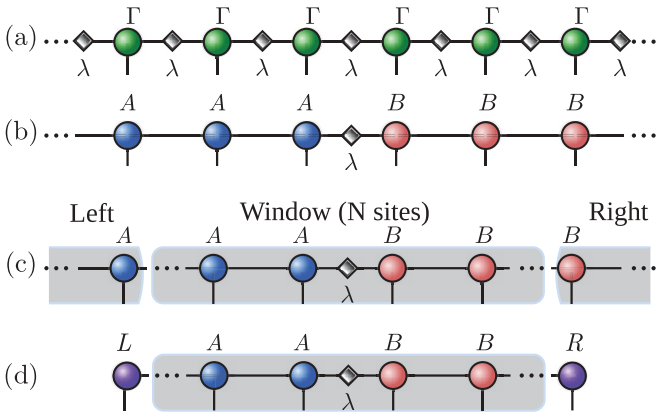

FIG. 1. (Color online) (a) Single-site translationally invariant canonical form iMPS. (b) One-site translationally invariant mixed canonical form iMPS. (c) Partition the whole chain into three parts: the left and right semi-infinite sublattices, and the middle part which is a window that contains N sites. (d) Finite-size MPS effectively represent the iMPS with left- and right-effective sites representing the left and right semi-infinite sublattices.

χ instead. χ plays a role as the refinement parameter of the iMPS. Specifically, the larger the χ the better the iMPS can represent the state. Diagrammatically, the iMPS is illustrated in Fig. 1(a) where a pair of tensors $\{\Gamma,\lambda\}$ is repeated at every lattice site throughout the whole infinite chain.

For convenience and later use, we can also rewrite Eq. (1) in the mixed canonical representation [see Fig. 1(b)] as

$$|\Psi\rangle = \sum_{s} \ldots A^{s_{i-1}} A^{s_i} \lambda B^{s_{i+1}} B^{s_{i+2}} \ldots |\mathbf{s}\rangle, \qquad (2)$$

where $A = \lambda\Gamma$ and $B = \Gamma\lambda$ satisfy the left and right canonical form constraints as follows:

$$\sum_{s_i} A^{s_i\dagger} A^{s_i} = \sum_{s_i} \Gamma^{s_i\dagger} \rho^R \Gamma^{s_i} = \mathbb{I}, \qquad (3)$$

$$\sum_{s_i} B^{s_i} B^{s_i\dagger} = \sum_{s_i} \Gamma^{s_i} \rho^L \Gamma^{s_i\dagger} = \mathbb{I}. \qquad (4)$$

In the above equations, ρ^R and ρ^L are nothing but the right and left reduced density matrices of the spin chain and defined as

$$\rho^L = \sum_{\alpha=1}^{\chi} (\lambda_\alpha)^2 \left|\Phi_\alpha^L\right\rangle \otimes \left\langle\Phi_\alpha^L\right|, \qquad (5)$$

$$\rho^R = \sum_{\alpha=1}^{\chi} (\lambda_\alpha)^2 \left|\Phi_\alpha^R\right\rangle \otimes \left\langle\Phi_\alpha^R\right|, \qquad (6)$$

where $|\Phi_\alpha^L\rangle$ and $|\Phi_\alpha^R\rangle$ are the left and right Schmidt vectors that are orthonormal.

The advantage of representing the MPS in the canonical form is that it not only fixes the gauge freedom in the MPS representation, which would otherwise cause numerical difficulties, but it is also very convenient for simplifying the computation of observables of an infinite system. In addition, the canonical form representation of iMPS is necessary in the truncation step of time evolution algorithms (both imaginary- and real-time evolution).

Now, let us partition the whole infinite-size spin chain into three parts as illustrated in Fig. 1(c). The middle part, called

the window, contains N sites of the spin chain and the two other parts contain left and right semi-infinite spin chains attached to this window. Then instead of considering a large number of tensors outside of the window of the iMPS we only use two matrices L and R that represent the whole left and right semi-infinite chains, where each has dimension $\chi \times \chi$, Fig. 1(d). These two matrices represent two boundary sites attached to the window, and are defined as the infinite boundaries of the finite spin chain.

We have already introduced the idea of shrinking the infinite spin chain to a finite spin chain with infinite boundary conditions. These infinite boundary conditions will have to capture all the properties of the infinite system. Although the idea of shrinking the infinite spin chain is quite simple, it is more complicated to realize. Specifically, we need to be sure that our finite-size system with infinite boundary conditions will behave similarly to the initial infinite system. To achieve this we require the effective Hamiltonian representing the infinite system, written in the basis of the finite MPS.

B. Effective Hamiltonian

Suppose that the total Hamiltonian of the initial infinite spin chain can be decomposed into five components, written as

$$H = H_L + H_{LW} + H_W + H_{WR} + H_R, \tag{7}$$

where H_L and H_R are the Hamiltonian components for the left and right semi-infinite spin chain, H_{LW} (H_{WR}) is the interaction term at the left (right) boundary of the window, respectively, and finally H_W is the Hamiltonian for the window with N sites.

As we do not consider the whole infinite spin chain, we do not need the full information contained in the Hamiltonian. Instead, we introduce the infinite boundary conditions to shrink the infinite chain to the finite chain. The Hamiltonian for this finite chain will be effectively described in the same way, as follows:

$$\tilde{H} = \tilde{H}_L + \tilde{H}_{LW} + H_W + \tilde{H}_{WR} + \tilde{H}_R, \tag{8}$$

where the tilde symbol is added in order to distinguish between the effective Hamiltonian and the full Hamiltonian of the system. We can see that H_W is the same in both Eq. (7) and Eq. (8). Our task is to find the effective Hamiltonians of the left and right semi-infinite chain and their interaction components with the window [the components in Eq. (8) with the tilde symbol].

We now show the method to calculate the effective Hamiltonian by using spin-1 isotropic antiferromagnetic Heisenberg model as an example. The Hamiltonian contains nearest-neighbor interaction terms as follows:

$$H = \sum_i \vec{S}_i \cdot \vec{S}_{i+1}, \tag{9}$$

where $\vec{S} = (S^x, S^y, S^z)$ is the vector containing matrices for the spin-1 representation of the spin algebra.

The effective Hamiltonian can now be written as

$$\tilde{H} = \tilde{H}_L + \tilde{\vec{S}}_L \cdot \vec{S}_1 + \sum_{i=1}^{N-1} \vec{S}_i \cdot \vec{S}_{i+1} + \vec{S}_N \cdot \tilde{\vec{S}}_R + \tilde{H}_R. \tag{10}$$

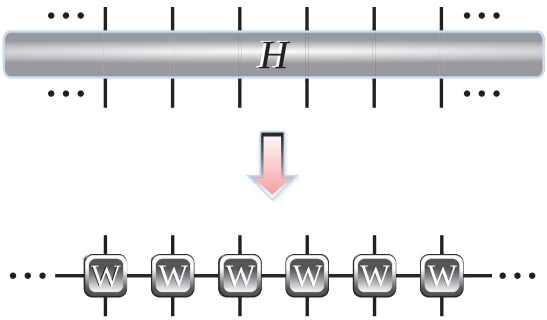

FIG. 2. (Color online) The full Hamiltonian of the system is decomposed into the tensor product of local matrix product operators.

We need to find the left and right effective Hamiltonians $\tilde{H}_L, \tilde{H}_R$ and also operators $\tilde{\vec{S}}_L, \tilde{\vec{S}}_R$ which are $\chi \times \chi$ matrices. The procedure to obtain the effective Hamiltonian is described in detail in Ref. 27, and we now briefly review it here.

Let us introduce the infinite matrix product operator (iMPO) which has the following form for an infinite-size spin chain:

$$\langle \sigma | H | \sigma' \rangle = \ldots W^{s_i s_i'} W^{s_{i+1} s_{i+1}'} \ldots, \tag{11}$$

where we denote $|\sigma\rangle = |\ldots s_i, s_{i+1} \ldots\rangle$ as the basis of the system. As the unit cell of this model contains a single site, the iMPO is represented by the same matrices $W^{ss'}$ repeated at every site of the chain; see Fig. 2.

With each type of Hamiltonian there are several ways to construct the iMPO; here we are using the method proposed in Ref. 21 where all the matrices are in lower triangular forms. For the Hamiltonian described by Eq. (9), these matrices have the following form:

$$W = \begin{bmatrix} \mathbb{I} & 0 & 0 & 0 & 0 \\ S^x & 0 & 0 & 0 & 0 \\ S^y & 0 & 0 & 0 & 0 \\ S^z & 0 & 0 & 0 & 0 \\ 0 & S^x & S^y & S^z & \mathbb{I} \end{bmatrix},$$

where $\mathbb{I}$ is a 3×3 identity matrix.

We now review the scheme proposed in Ref. 27 to find all the left effective operators; a similar scheme can be applied for the right operators. Specifically, we need to find the dominant eigenvector of the transfer matrix diagrammatically illustrated in Fig. 3(a). This dominant eigenvector contains five components, $\vec{E} = (E_1, E_2, E_3, E_4, E_5)$. As we will see later, this dominant eigenvector contains the information of the left effective Hamiltonian that we need, or in DMRG terminology, $\vec{E}$ is the vector of block operators describing the effective Hamiltonian. However, as the transfer matrix is not diagonalizable, we need to find all the elements of $\vec{E}$ independently by employing the recursion relation, see Fig. 3(c), which reads

$$E_\alpha(n+1) = T_{W_{\alpha\alpha}}(E_\alpha(n)) + \sum_{\beta > \alpha} T_{W_{\beta\alpha}}(E_\beta(n)), \tag{12}$$

where we have defined

$$T_X(E) = \sum_{ss'} \langle s | X | s' \rangle A^{s'\dagger} E A^s, \tag{13}$$

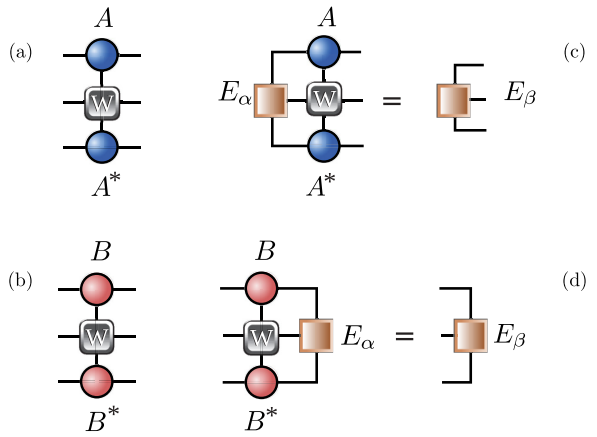

FIG. 3. (Color online) (a) Generalized transfer matrix for finding the left dominant eigenvector $\vec{E}$. (b) Generalized transfer matrix for finding the right dominant eigenvector $\vec{E}$. (c) Equation to find left dominant eigenvector. (d) Equation to find right dominant eigenvector.

which is the generalized transfer operator to include a local operator X acting on the physical degree of freedom of the MPS. The relevant local operators will be obtained from the elements of the MPO matrix $W_{\beta\alpha}$, and we make use of the fact that W is lower triangular to restrict the summation to $\beta \geqslant \alpha$. Since the other terms $S_{\beta\alpha}$ with $\beta < \alpha$ are equal to zero, we can solve immediately the recursion relation Eq. (12) for the last component, in this example being E_5,

$$\begin{aligned} E_5(n+1) &= T_{W_{55}}(E_5(n)) \\ &= \sum_{ss'} \langle s|\mathbb{I}|s'\rangle A^{s'\dagger} E_5(n) A^s, \end{aligned} \tag{14}$$

which implies that in the large-n limit $E_5(n)$ is the eigenvector of the transfer operator with largest eigenvalue. If the iMPS is in the canonical form then this largest eigenvalue will be 1 and we have

$$E_5 = \tilde{\mathbb{I}}, \tag{15}$$

where $\tilde{\mathbb{I}}$ is a $\chi \times \chi$ identity matrix. Moving on to E_4, we have

$$\begin{aligned} E_4(n+1) &= \underbrace{T_{W_{44}}(E_4(n))}_{0} + \sum_{ss'} \langle s|S^z|s'\rangle A^{s'\dagger} \underbrace{E_5(n)}_{\tilde{\mathbb{I}}} A^s \\ &= \sum_{ss'} \langle s|S^z|s'\rangle A^{s'\dagger} A^s = \tilde{S}^z_L, \end{aligned} \tag{16}$$

and here the fact that the diagonal matrix element $W_{44} = 0$ implies that the solution for E_4 is simply a function of E_5 and local operators. Similarly,

$$\begin{aligned} E_3(n+1) &= \underbrace{T_{W_{33}}(E_3(n))}_{0} + \sum_{ss'} \langle s|S^y|s'\rangle A^{s'\dagger} \underbrace{E_5(n)}_{\tilde{\mathbb{I}}} A^s \\ &= \sum_{ss'} \langle s|S^y|s'\rangle A^{s'\dagger} A^s = \tilde{S}^y_L, \end{aligned} \tag{17}$$

$$\begin{aligned} E_2(n+1) &= \underbrace{T_{W_{22}}(E_2(n))}_{0} + \sum_{ss'} \langle s|S^x|s'\rangle A^{s'\dagger} \underbrace{E_5(n)}_{\tilde{\mathbb{I}}} A^s \\ &= \sum_{ss'} \langle s|S^x|s'\rangle A^{s'\dagger} A^s = \tilde{S}^x_L, \end{aligned} \tag{18}$$

and finally, the most complicated term that contains the effective Hamiltonian of the left semi-infinite spin chain is determined as

$$\begin{aligned} E_1(n+1) &= T_{W_{11}}(E_1(n)) + \sum_{\beta>1} T_{W_{\beta 1}}(E_\beta(n)) \\ &= \sum_{ss'} \langle s|\mathbb{I}|s'\rangle A^{s'\dagger} E_1(n) A^s \\ &\quad + \sum_{ss'} \langle s|S^x|s'\rangle A^{s'\dagger} \underbrace{E_2(n)}_{\tilde{S}^x_L} A^s \\ &\quad + \sum_{ss'} \langle s|S^y|s'\rangle A^{s'\dagger} \underbrace{E_3(n)}_{\tilde{S}^y_L} A^s \\ &\quad + \sum_{ss'} \langle s|S^z|s'\rangle A^{s'\dagger} \underbrace{E_4(n)}_{\tilde{S}^z_L} A^s. \end{aligned} \tag{19}$$

We can also write this equation in a compact form as

$$E_1(n+1) = \sum_{ss'} \langle s|\mathbb{I}|s'\rangle A^{s'\dagger} E_1(n) A^s + C, \tag{20}$$

where C is a constant that is defined as the summation of last three terms in Eq. (19). Our task is to solve Eq. (20). To see how this is done, let us assume the initial solution $E_1(0) = 0$. This is an arbitrary choice that has no effect on the final solution, up to an irrelevant constant. Then,

$$\begin{aligned} E_1(1) &= C, \quad E_1(2) = T_{\mathbb{I}}(C) + C, \\ E_1(3) &= T_{\mathbb{I}}(T_{\mathbb{I}}(C) + C) + C \\ &= T_{\mathbb{I}}(T_{\mathbb{I}}(C)) + T_{\mathbb{I}}(C) + C, \\ &\cdots \end{aligned} \tag{21}$$

$$E_1(n+1) = T_{\mathbb{I}}(E_1(n)) + C. \tag{22}$$

In general we can write the solution as follows:

$$\begin{aligned} E_1(n) &= \sum_{k=0}^{n-1} T^k_{\mathbb{I}}(C) \\ &= C + T_{\mathbb{I}}(C) + T_{\mathbb{I}}(T_{\mathbb{I}}(C)) + T_{\mathbb{I}}(T_{\mathbb{I}}(T_{\mathbb{I}}(C))) + \cdots. \end{aligned} \tag{23}$$

This is the summation of a geometric series, which has the solution

$$\sum_{k=0}^{n-1} a x^k = \frac{a(1-x^n)}{1-x}. \tag{24}$$

In our case

$$\sum_{k=0}^{n-1} T^k_{\mathbb{I}}(C) = \frac{(\tilde{\mathbb{I}} - T^n_{\mathbb{I}})(C)}{(\tilde{\mathbb{I}} - T)(C)}. \tag{25}$$

Notice that the spectrum of transfer matrix $T_{\mathbb{I}}$ will contain the identity $\tilde{\mathbb{I}}$ and density matrix $\tilde{\rho}$ as a left/right eigenvector pair with eigenvalue 1. Therefore, this summation will be diverging. To avoid this, let us decompose the summation into two terms as

$$E_1(n) = \tilde{H}_L + e_0 n \tilde{\mathbb{I}}, \tag{26}$$

where $\tilde{H}_L$ contains all the terms that are perpendicular to the identity (meaning $\mathrm{tr}\tilde{H}_L\rho = 0$) and is actually the effective Hamiltonian of the left semi-infinite chain; e_0 is a constant equal to the energy per site of the infinite chain. Note that $\tilde{H}_L$ removes the constant contribution of the energy that would diverge in the thermodynamic limit. Now we can check the recursion relation by substituting Eq. (26) into Eq. (22); we have

$$\tilde{H}_L + e_0(n+1)\tilde{\mathbb{I}} = T_{\mathbb{I}}(\tilde{H}_L) + T_{\mathbb{I}}(e_0 n\tilde{\mathbb{I}}) + C. \quad (27)$$

This simplifies to a linear equation for $\tilde{H}_L$,

$$(\tilde{\mathbb{I}} - T_{\mathbb{I}})(\tilde{H}_L) = C - e_0\tilde{\mathbb{I}}, \quad (28)$$

where $e_0 = \mathrm{Tr}(\rho C)$ (ρ is density matrix). By solving this linear equation we find the effective Hamiltonian $\tilde{H}_L$ and this completes the vector of block operators $E_\alpha(n)$. Note that the energy per site contribution $e_0 n\tilde{\mathbb{I}}$ is a constant shift in the energy and is therefore irrelevant for most purposes.

In summary, we have explained in this section how to obtain the effective Hamiltonian on the left of the window. Specifically, we have obtained $\tilde{H}_L = E_1$ and also operators $\tilde{\vec{S}}_L = \{\tilde{S}^x_L, \tilde{S}^y_L, \tilde{S}^z_L\} = \{E_2, E_3, E_4\}$. For the right effective Hamiltonian, a completely similar procedure is performed. In the next section we will use this calculation to investigate the problem of real-time evolution of iMPS in the presence of local perturbation.

III. APPLICATION: REAL-TIME EVOLUTION OF iMPS IN THE PRESENCE OF LOCAL PERTURBATION

We now apply the procedure for finding the effective Hamiltonian and the infinite boundary conditions proposed above to study dynamical properties of an infinite spin chain in the presence of a local perturbation. As an infinite MPS will be effectively represented by a finite MPS, we can apply a standard MPS time-evolution technique to study the reaction of the infinite system to a local perturbation. The MPS technique that we use here is the TEBD algorithm.

A. Local perturbation

We wish to take an infinite spin chain which is in its ground state, and perturb locally one site. Suppose that we have already found the ground state of the system (for example, by iDMRG or iTEBD), represented by a translationally invariant iMPS with a one- or two-site unit cell; the wave function $|\Psi_{GS}\rangle$ is written as in Eq. (2). Then we choose one site and perturb it locally by flipping the spin of that site with flipping spin operators S^+ (flip spin up) or S^- (flip spin down). The system is not in the ground state anymore, but a mixture of excited states, and is no longer described by a translationally invariant iMPS. Let us flip the spin at a certain position j in the chain and define a new state as

$$|\tilde{\Psi}\rangle = S^+_j|\Psi_{GS}\rangle. \quad (29)$$

As a result of spin flipping, a wave packet is formed centered at the flipped spin. As an illustration using the spin-1 isotropic antiferromagnetic Heisenberg model, in Fig. 4, we plot the local magnetization of the system after flipping one spin in the middle of the chain. We can see that a wave packet is formed with the peak located in the middle site. The amplitude of this wave packet decreases when moving away from the middle point. The width of the wave packet depends on the correlation length of the system. Note however that despite the breaking of translational invariance at long range, only one tensor of the MPS is different from that of the translationally invariant ground state.

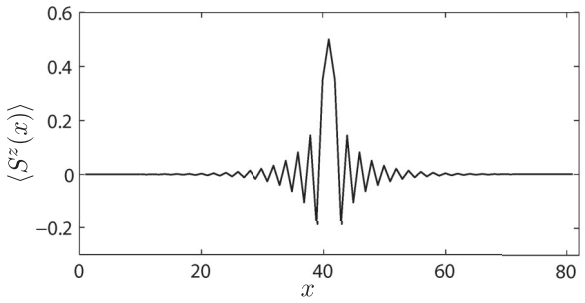

FIG. 4. The wave packet (local magnetization) is formed after flipping one spin in the middle of the chain. The result is obtained by using a two-site translationally invariant iMPS for the ground state with bond dimension $\chi = 160$.

B. Real-time evolution

Let us now study real-time evolution of an infinite spin chain. The initial state of the system is a locally perturbed state $|\tilde{\Psi}(0)\rangle$. This state will evolve in time and is described by the solution of the Schrödinger equation

$$|\tilde{\Psi}(t)\rangle = e^{-i\tilde{H}t}|\tilde{\Psi}(0)\rangle. \quad (30)$$

As mentioned above, this state can be effectively represented by a finite MPS containing $N+2$ sites where the perturbed site is in the middle of the chain at site $i = N/2$, with an effective Hamiltonian $\tilde{H}$ describing the finite system. The two boundary sites are now represented by the boundary tensors L^α and R^β, which are the usual boundary sites of a finite MPS with dimensions $1 \times \chi$ and $\chi \times 1$ respectively, except now the local Hilbert space is the χ-dimensional effective Hilbert space for the left and right semi-infinite strips. In practice we do not actually need the L^α and R^β tensors as these are identity elements, $L^\alpha_i = \delta_{\alpha i}$ and $R^\beta_j = \delta_{\beta j}$, but their use allows us to formally write the state of the system Eq. (2) as a finite MPS,

$$|\tilde{\Psi}\rangle = \sum_{\{s_i\}} L^\alpha A^{s_1}_1 \lambda A^{s_2}_2 \ldots A^{s_N}_N R^\beta \, |\alpha, \tilde{\mathbf{s}}, \beta\rangle, \quad (31)$$

where $|\tilde{\mathbf{s}}\rangle = |s_1, s_2, \ldots s_N\rangle$. The location of the λ matrix will sweep through the system as usual in finite-size DMRG algorithms,[22] with all the tensors to the left of λ satisfying the the left canonical constraint of Eq. (3) and all the tensors on the right of λ matrix satisfying the right canonical constraint in Eq. (4). Note that it is not possible to write this system in the canonical Γ, Λ form used by Vidal[3] without modifying the boundary tensors L, R.

With an effective finite system representing the infinite system, we can proceed with the real-time evolution by employing the TEBD algorithm. Before continuing, we will briefly reiterate the main features of the TEBD algorithm. For more details, refer to the original work.[3] In this algorithm the

time evolution operator e^{-iHt} is decomposed as a product of M operators $e^{-iH\delta t}$ (where $\delta t \ll 1$ is the small time step and $M = t/\delta t$). In turn, each term $e^{-iH\delta t}$ is decomposed into products of local terms by using Suzuki-Trotter decomposition. Normally, the Hamiltonian is written as the summation of two terms. With the Hamiltonian just containing nearest-neighbor interaction terms, we can rewrite it in the following form:

$$H = H_{odd} + H_{even}, \tag{32}$$

where $H_{odd} = \sum_{oddi} h^{[i,i+1]}$ and $H_{even} = \sum_{eveni} h^{[i,i+1]}$. Terms in either H_{odd} or H_{even} commute with each other. However, the terms in H_{odd} do not commute with ones in H_{even} in general. Then the first-order Suzuki-Trotter decomposition of the time evolution operator at each time step δt is

$$\begin{aligned} e^{-iH\delta t} &= e^{-iH_{odd}\delta t} e^{-iH_{even}\delta t} + O(\delta t^2) \\ &= \bigotimes_{oddi} e^{-ih^{[i,i+1]}\delta t} \bigotimes_{eveni} e^{-ih^{[i,i+1]}\delta t} + O(\delta t^2). \end{aligned} \tag{33}$$

As a consequence of the nonzero commutation relation between the odd and even terms of the Hamiltonian, the Suzuki-Trotter decomposition will produce some error on the order of δt^2. However, this error can be controlled by using a small time step δt or by taking high-order decomposition.[30]

Here, we modify slightly the TEBD algorithm to investigate the real-time evolution of our locally perturbed system. Specifically, we do not need to find the inverse of the λ matrix after acting the two-body gate on a given link of two sites, but instead we use two more SVDs to shift the λ matrix by two sites to the next update link. This step is also important to get an optimal truncation which is essential for each local update. As a price of implementing two extra SVDs, this step may be a little bit costly. However, the big advantage of doing this is that we can avoid the inverse of λ that is numerically unstable.

For convenience and clarity, we write the time evolution operator with time step δt in the first order of Suzuki-Trotter decomposition:

$$\begin{aligned} e^{-i\tilde{H}\delta t} &= e^{-i(\tilde{H}_L+\tilde{H}_{LW}+H_W+\tilde{H}_R+\tilde{H}_{RW})\delta t} \\ &\cong e^{-i\tilde{H}_L\delta t} e^{-i\tilde{H}_{LW}\delta t} e^{-iH_W\delta t} e^{-i\tilde{H}_R\delta t} e^{-i\tilde{H}_{RW}\delta t} \\ &= U_L U_{LW} U_W U_R U_{RW}. \end{aligned} \tag{34}$$

The update scheme of real-time evolution at each time step is illustrated diagrammatically in Fig. 5 for an $N = 6$ window. However, in principle N can be any arbitrary finite number. Each time step includes two successive sweeps: one from the left to the right and vice versa. Note that with our specific choice of an even number of sites inside the window N the interaction terms on the left and right sides of the window are operationally equivalent to the even terms.

IV. RESULTS

By replacing the iMPS with an effective finite MPS containing two boundary sites we can evolve the locally perturbed ground state in time. Here we present the results computed for the spin-1 isotropic antiferromagnetic Heisenberg model. The initial ground state is represented by the iMPS with bond dimension $\chi = 160$ and is evolved to a state with maximum truncated bond dimension $\chi_C = 200$. Truncation

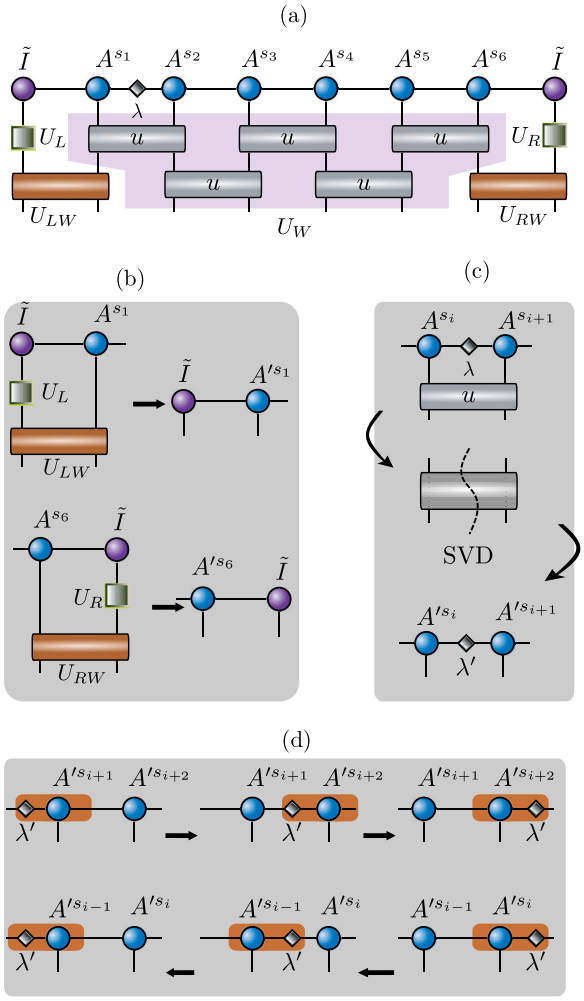

FIG. 5. (Color online) (a) Applying the operator $e^{-i\tilde{H}\delta t}$ to the effective finite MPS. (b) Update the left and right tensors by contracting tensors $\{U_L, U_{LW}, \tilde{I}, A^{s_1}\}$ and $\{U_R, U_{RW}, \tilde{I}, A^{s_6}\}$. (c) Update the new tensors when applying two-body gate u on the odd or even link. Contracting all the tensors involved and take the SVD of that. The bond dimension will increase after taking the SVD, so we need to do the truncation to keep new tensors $A'^{s_i}, A'^{s_{i+1}}$, and λ' in the desired bond dimension. (d) Shifting λ' to the right (or left) of the updated link if sweeping direction is from left to right (or right to left) by taking two successive SVDs.

error is approximately equal to 10^{-7}. After flipping the central spin, the system is evolved up to time $t = 30$ where time step $\delta t = 0.05$ is used for the fourth-order Suzuki-Trotter decomposition.

A. Wave packet propagating in time

In order to understand how the wave packet is propagating in the effective finite MPS where the infinite boundaries are present, we compute the local magnetizations in time at each site of the spin chain. The result is shown in the Fig. 6. For the system with window size $N = 60$, as we can see, the wave packet at the beginning is formed at the middle of the chain and then spreads out. Importantly, what we can see here is that when the wave front hits the infinite boundaries, there is no back reflection or counterpropagating effect; it passes through

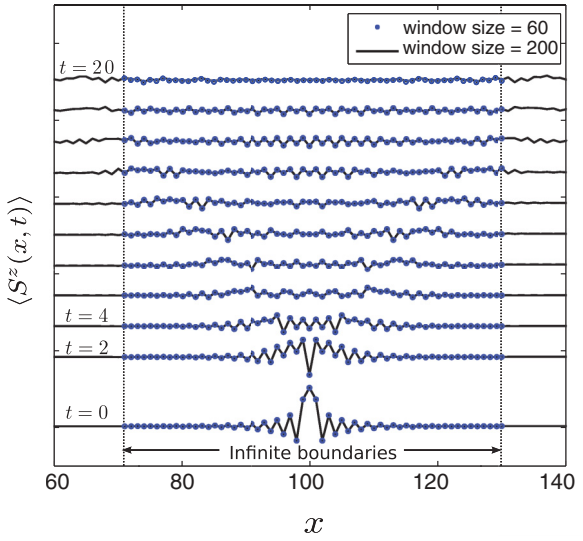

FIG. 6. (Color online) Wave packet propagates in time with window size $N = 60$ (blue dots). The window is expanded to $N = 200$ (black solid lines) after simulation to see how the wave front propagates beyond the infinite boundaries.

the boundaries. This can be verified when we look at how the wave packet propagates outside the window in the effective Hilbert space. Specifically, we expand the window after the simulation by inserting the original orthogonal tensors A and B at the edges. From this we calculate expectation values outside the original window. From Fig. 6 we can see that when the window is expanded to window size $N = 200$, the wave front moves smoothly to the exterior, justifying our approach.

Now, for comparison, we also plot the propagation of the wave packet in time with different window sizes. These windows have sizes fixed from the beginning of the real-time evolution. As we can see from Fig. 7, the wave packets of different window sizes are coincident with each other in the middle region of the plot. This is exemplified in Fig. 8(a), where we plot the error in the magnetization at the site of the perturbation as a function of time t, for window sizes 60, 100,

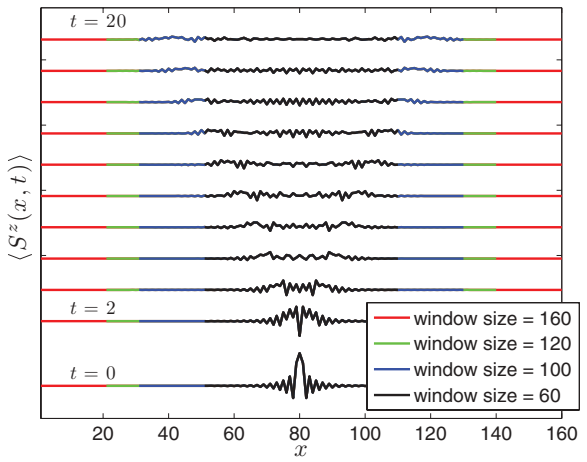

FIG. 7. (Color online) Wave packet propagates in time with different window sizes which are fixed at the beginning of real-time evolution. The lines are distinguishable in the center of the plot.

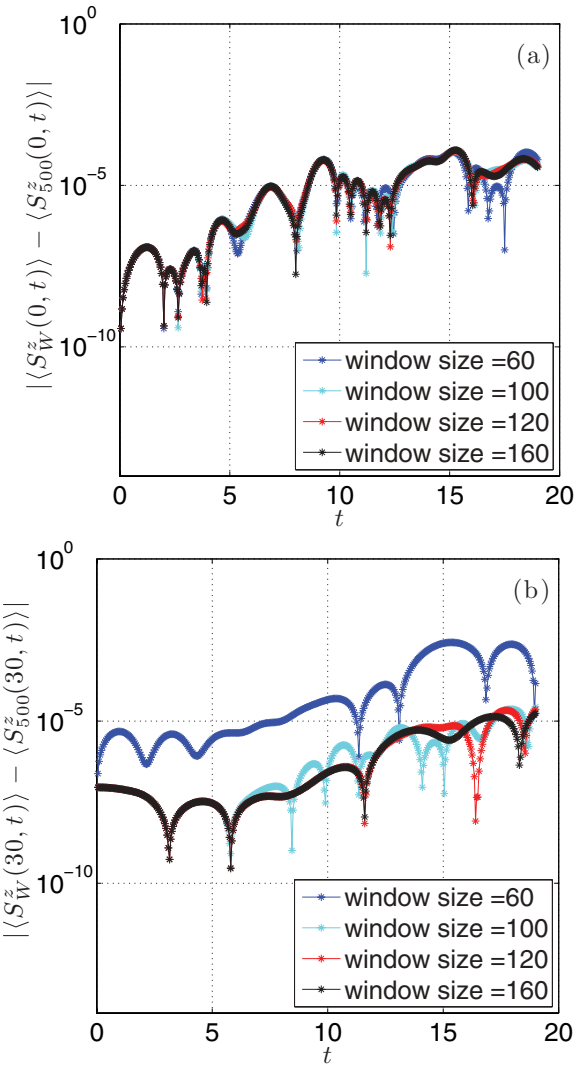

FIG. 8. (Color online) Comparisons of the differences of local magnetization in time at a fixed site x_i between window sizes $N = \{60, 100, 120, 160\}$ and a highly accurate calculation using a 500-site finite chain. (a) Perturbed point of chain $x_i = 0$. (b) Boundary point of the chain $x_i = 30$.

120, 160. The curves are nearly coincident, showing that the dominant contribution to the error is from the Suzuki-Trotter decomposition, not the finite window. Figure 8(b) shows the error in the magnetization 30 sites away. If the window is larger than 60 sites, then we again see no error beyond the usual Suzuki-Trotter error. For the 60-site window, the site where we measure the magnetization corresponds to the edge of the window and in this calculation the error is somewhat increased, even at very small times, which is probably due to a slight mismatch of using a slightly different approximation for the time evolution operator inside the window (Suzuki-Trotter) and outside the window (direct calculation of the exponential of the effective Hamiltonian). Nevertheless, there is no sign of any significant increase in the relative error due to the wave front passing through the edge of the window and into the infinite boundary tensor. Indeed, the leading edge of the wave front passes site 30 at around $t = 10$, and by $t = 18$ the entire wave front has already passed.

B. Unequal-time two-point correlator and spectral function

Let us define an unequal-time two-point correlator as

$$A(x,t) = \langle\phi|S_x^-(t)S_{x_M}^+(0)|\phi\rangle, \tag{35}$$

where the subscripts in spin-flip operators indicate positions of the chain and x_M is the middle position; $|\phi\rangle$ is the initial state of the system that we want to evolve. This equation is equivalent with

$$A(x,t) = e^{iE_G t}\langle\phi|S_x^-(0)|\psi(t)\rangle, \tag{36}$$

in which we have already replaced $S_x^-(t) = e^{iHt}S_x^-(0)e^{-iHt}$ and $|\psi(t)\rangle = e^{-iHt}S^+(0)|\phi\rangle$. We also have a phase factor appear in Eq. (36) due to $|\phi\rangle$ being the eigenvector of the Hamiltonian H corresponding to the eigenvalue E_G. Obviously, the unequal-time two-point correlator $A(x,t)$ can be calculated easily, as the time-evolved state $|\psi(t)\rangle$ can be obtained quickly from the scheme proposed above for evolving the locally perturbed state.

From the unequal time two-point correlator we construct the Green's function that is defined as

$$G(x,t) = -iA(x,t). \tag{37}$$

Figure 9 shows the plots of the real and imaginary parts of the Green's function for the system with window size $N = 60$. As we can see, there are wave fronts propagating from the middle point toward the infinite boundaries. Again, there is no back reflection of the wave front at the boundaries.

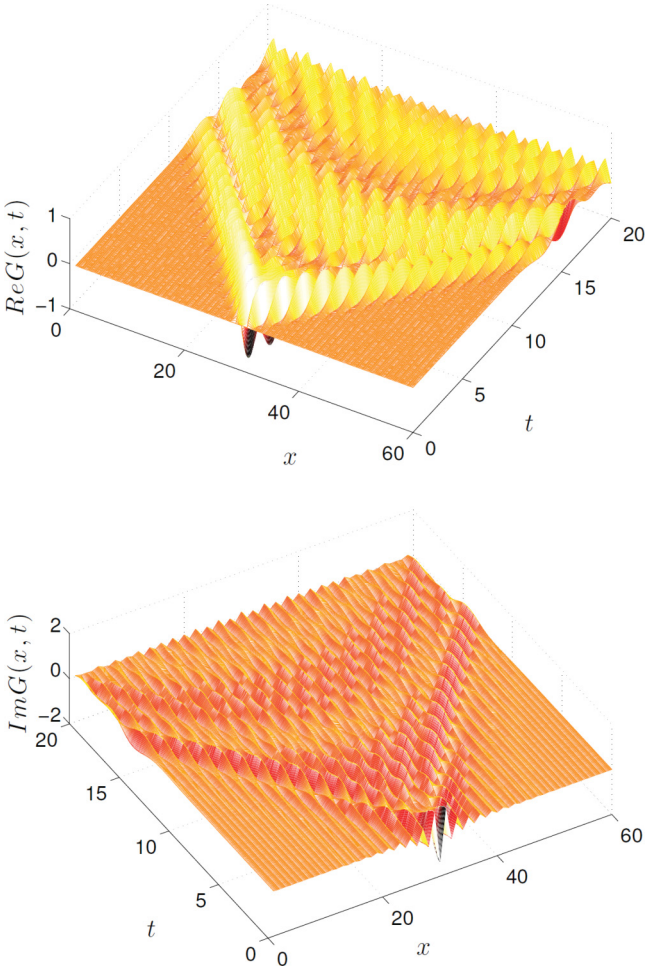

FIG. 9. (Color online) Plots of the real and imaginary parts of the Green's function versus time and spin chain space.

By Fourier transforming of the Green's function into momentum and frequency spaces, we can extract the spectrum of the lattice system. Specifically, the Fourier transform of $G(x,t)$ is

$$G(q,\omega) = \int_{-\infty}^{\infty} dt e^{i\omega t}\sum_x e^{-iqx}G(x,t). \tag{38}$$

For the case of the spin-1 isotropic antiferromagnetic Heisenberg model, the Green's function is even in x and t, and we can simplify Eq. (38) as follows:

$$G(q,\omega) = \int_{-\infty}^{\infty} dt\cos\omega t\sum_x \cos qxG(x,t). \tag{39}$$

$G(x,t)$ is a continuous function in time t. However, in our simulation, we have already discretized the time into the small time steps δt. Therefore, Eq. (39) can be written as

$$G(q,\omega) \approx 2\sum_{t=0}^{T_{max}}\cos\omega t\sum_x \cos qxG(x,t). \tag{40}$$

The spectral function is now defined as

$$S(q,\omega) = -\frac{1}{\pi}\mathrm{Im}G(q,\omega). \tag{41}$$

Note that as we have already introduced the infinite boundaries for our finite MPS, the wave front can now propagate freely

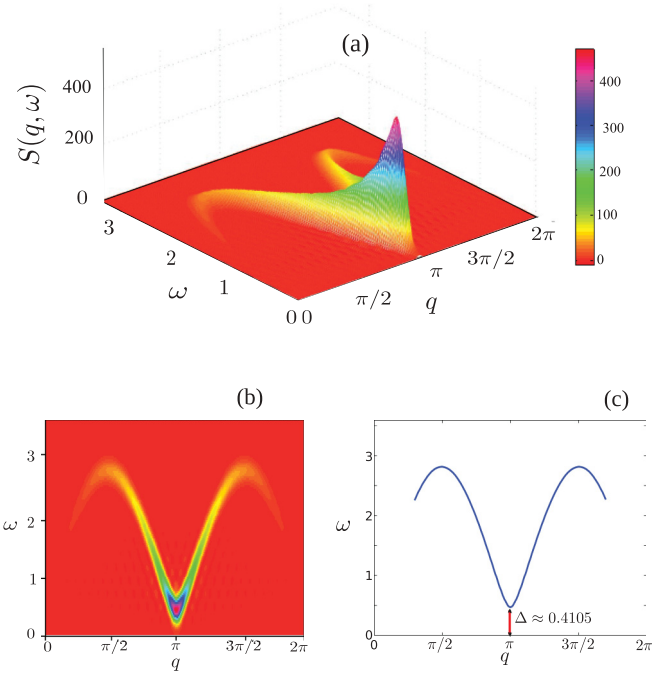

FIG. 10. (Color online) (a) Spectral function versus momentum and frequency for the spin-1 isotropic Heisenberg model; the window is $N = 60$. (b) Spectrum viewed from the top when it is projected on the (ω,q) plane. (c) The dispersion relation is derived from the maximum of the spectrum.

through these boundaries without any back reflection. In principle, in obtaining the spectral function we do not need to have any cutoff in time to keep the available data. In Fig. 10(a), we plot the spectral function versus momentum and frequency. In order to get a smooth spectrum, we have multiplied $G(x,t)$ with a Gaussian window function of the form $\exp[-4(t/T)^2]$ as introduced in Ref. 8. By viewing from the top of this figure, we can see the dispersion relation appears very clearly in Fig. 10(b). Collecting the data pairs (ω,q) that correspond to the maximum of spectrum and plotting them, we can see the dispersion relation of the system appears nicely in Fig. 10(c). The value of the gap at $q = \pi$ measured in our simulation is $\Delta = 0.4105$, consistent with the value found in Ref. 8. Thus using the method we have presented here we obtain a spectral function with comparable accuracy to previous calculations but with significantly reduced computational effort.

V. CONCLUSIONS

We have introduced the infinite boundary condition as a procedure for representing a finite section of a lattice embedded within an infinite chain. With just two boundary sites we can describe the relevant information for the whole semi-infinite spin chain. Therefore, instead of simulating the iMPS, we just need the finite MPS with two additional effective sites. This helps to greatly reduce the computational cost as well as computer memory in simulating the infinite system where the MPS cannot be represented by translationally invariant tensors. After finding the effective Hamiltonian and operators associated with the infinite boundary, the numerical algorithms we use are straightforward, variants of the well-known MPS/DMRG algorithms for finite-size systems. Hence the general procedure is applicable to a wide variety of problems.

As an example for possible application we considered the real-time evolution of the 1D spin-1 isotropic Heisenberg model. The initial state of the system is the ground state where one central site is locally perturbed. As a result, a wave packet is formed and spreads out from the center in time. As we have already attached the infinite boundaries to the finite system, we do not need to end the simulation when the wave front hits the boundaries, as useful information can be still be obtained, at least for short time intervals, as the degrees of freedom propagate into the boundary tensor. The resulting spectral function and dispersion relation compare well with previous investigations. The gap value we obtained compares well with that obtained in Ref. 8, although smaller window size and longer evolution time are used. In fact, there is no restriction in our method which says that the window size must remain constant throughout the calculation. Expanding the window size is straightforward, as the tensors representing the system outside the window are translationally invariant anyway, so additional tensors simply need to be orthogonalized and incorporated into the finite window. Similarly, reducing the size of the window is achieved by incorporating tensors from the finite window into the infinite boundary tensors, which is a simple tensor contraction for the new effective Hamiltonian and associated operators. The use of these techniques is described in Ref. 32.

We have described the procedure for infinite boundary conditions for a one-dimensional matrix product state; however the general procedure is applicable to any regular tensor network. In particular, this method is directly applicable to iPEPS.[16–18] This may be an effective way to obtain the spectral function of a 2D system, among many other possible applications.

We have recently learned of some related works.[33,34]

ACKNOWLEDGMENTS

We acknowledge support from the Australian Research Council Centre of Excellence for Engineered Quantum Systems and the Discovery Projects funding scheme (Project No. DP1092513).

[1] S. R. White, Phys. Rev. Lett. **69**, 2863 (1992).
[2] S. R. White, Phys. Rev. B **48**, 10345 (1993).
[3] G. Vidal, Phys. Rev. Lett. **91**, 147902 (2003).
[4] G. Vidal, Phys. Rev. Lett. **93**, 040502 (2004).
[5] S. Ostlund and S. Rommer, Phys. Rev. Lett. **75**, 3537 (1995).
[6] M. Fannes, B. Nachtergaele, and R. Werner, Commun. Math. Phys. **144**, 443 (1992).
[7] D. Perez-Garcia, F. Verstraete, M. M. Wolf, and J. I. Cirac, Quantum Inf. Comput. **7**, 401 (2007).
[8] S. R. White and A. E. Feiguin, Phys. Rev. Lett. **93**, 076401 (2004).
[9] A. J. Daley, C. Kollath, U. Schollwoeck, and G. Vidal, J. Stat. Mech.: Theor. Exp. (2004) P04005.
[10] T. Nishino, K. Okunishi, Y. Hieida, N. Maeshima, and Y. Akutsu, Nucl. Phys. B **575**, 504 (2000).
[11] T. Nishino, Y. Hieida, K. Okunishi, N. Maeshima, Y. Akutsu, and A. Gendiar, Prog. Theor. Phys. **105**, 409 (2001).
[12] A. Gendiar, N. Maeshima, and T. Nishino, Prog. Theor. Phys. **110**, 691 (2003).
[13] N. Maeshima, Y. Hieida, Y. Akutsu, T. Nishino, and K. Okunishi, Phys. Rev. E **64**, 016705 (2001).
[14] Y. Nishio, N. Maeshima, A. Gendiar, and T. Nishino, arXiv:cond-mat/0401115.
[15] A. Gendiar, T. Nishino, and R. Derian, Acta Phys. Slov. **55**, 141 (2005).
[16] F. Verstraete and J. I. Cirac, arXiv:cond-mat/0407066.
[17] V. Murg, F. Verstraete, and J. I. Cirac, Phys. Rev. A **75**, 033605 (2007).
[18] J. Jordan, R. Orus, G. Vidal, F. Verstraete, and J. I. Cirac, Phys. Rev. Lett. **101**, 250602 (2008).
[19] G. Vidal, Phys. Rev. Lett. **98**, 070201 (2007).
[20] R. Orús and G. Vidal, Phys. Rev. B **78**, 155117 (2008).
[21] I. P. McCulloch, arXiv:0804.2509.
[22] I. P. McCulloch, J. Stat. Mech. (2007) P10014.
[23] G. M. Crosswhite, A. C. Doherty, and G. Vidal, Phys. Rev. B **78**, 035116 (2008).

[24]V. Mung, J. I. Cirac, B. Pirvu, and F. Verstraete, New J. Phys. **12**, 025012 (2010).
[25]Chen Liu, Ling Wang, Anders W. Sandvik, Yu-Cheng Su, and Ying-Jer Kao, Phys. Rev. B **82**, 060410(R) (2010).
[26]S. R. White and I. Affleck, Phys. Rev. B **77**, 134437 (2008).
[27]L. Michel and I. P. McCulloch, arXiv:1008.4667.
[28]J. Haegeman, B. Pirvu, D. J. Weir, J. I. Cirac, T. J. Osborne, H. Verschelde, and F. Verstraete, Phys. Rev. B **85**, 100408(R) (2012).
[29]M. C. Bañuls, M. B. Hastings, F. Verstraete, and J. I. Cirac, Phys. Rev. Lett. **102**, 240603 (2009).
[30]N. Hatano and M. Suzuki, arXiv:math-ph/0506007.
[31]J. A. Kjäll, F. Pollmann, and J. E. Moore, Phys. Rev. B **83**, 020407 (2011).
[32]H. N. Phien, G. Vidal, and I. P. McCulloch, arXiv:1207.0678.
[33]V. Zauner, M. Ganahl, H. G. Everts, and T. Nishino, arXiv:1207.0862.
[34]A. Milsted, J. Haegeman, T. J. Osborne, and F. Verstraete, arXiv:1207.0691.